

1 Separation of surface flow from subsurface flow in catchments using runoff 2 coefficient

3
4 A. Afshar Ardekani¹, T. Sabzevari^{1*}, A. Torabi Haghighi², A. Petroselli³

5 [1] Department of Civil Engineering, Islamic Azad University, Estahban Branch , Fars, Iran

6 [2] Water, Energy and Environmental Engineering Research Unit, University of Oulu, Finland

7 [3] Department of Economics, Engineering, Society and Business Organization (DEIM), Tuscia University, Via S.
8 Camillo de Lellis snc, 01100 Viterbo (VT), Italy.

9 * Corresponding Author: t_sabzevari@iauest.ac.ir, tooraj.sabzevari@gmail.com

10 11 **Abstract:**

12 Separating surface flow (SF) from subsurface flow (SSF) based on direct runoff
13 measurements in river gauges is an important issue in hydrology. In this study, we
14 developed a simple and practical method, based on runoff coefficient (RC), for
15 separating SF from SSF. RC depends mainly on soil texture, land use and land cover,
16 but we also considered the effect of slope and rainfall intensity. We assessed our
17 RC-based method for three different soil types by comparing the value obtained with
18 laboratory rainfall simulator data. The correlation coefficient between observed and
19 calculated data exceeded 0.93 and 0.63 when estimating SF and SSF respectively.
20 The method was then used to separate SF and SSF in two catchments (Heng-Chi and
21 San-Hsia) in Northern Taiwan, and the results were compared with those produced
22 by the geomorphological instantaneous unit hydrograph (GIUH) model. Test
23 revealed that, if RC is calculated accurately, the proposed method can satisfactorily
24 separate SF from SSF at catchment scale.

25 **Key Words:** Surface flow, Subsurface flow, Separation, Runoff coefficient

26 **1. Introduction**

27 Estimating direct runoff is important in flood risk assessment and in the design of
28 hydraulic structures such as diversion and storage dams. In general, total runoff
29 occurring in streams consists of three components: surface runoff, subsurface flow,
30 and base flow. The sum of surface runoff and subsurface flow is commonly defined
31 as direct runoff.

32 Surface runoff (SF) is usually the most important of such three components. Many
33 rainfall-runoff models have been proposed to compute the surface flow of ungauged
34 catchments (Menberu et al , 2014, Sabzevari, 2017; Keshtkaran et al, 2018; Petroselli
35 et al, 2020a, b; Dehghanian et al, 2020).

36 However, in hilly catchments with very permeable soil or dense vegetation cover,
37 the rate of infiltration is high and can lead to rapid subsurface flow. In such
38 catchments, subsurface flow can enter streams at the lower part of hillslopes and
39 contribute effectively to direct flow (Singh, 1988 , Sabzevari et al, 2013).

40 The underground flow can be slow or quick. The quick underground flow is often
41 called saturated subsurface flow (SSF), and it usually occurs near the soil surface,
42 eventually entering the streams. Slow underground flow is generally a source of
43 groundwater recharge. It is formed through infiltration of water into deeper layers of
44 the soil and eventually enters rivers as base flow (BF).

45 Based on the Dunne-Black runoff mechanism, the lower soil layers are saturated by
46 SSF, which eventually joins surface flow (SF) entering the streams (Chow et al.
47 1988). To separate SF from SSF, the complicated interactions of saturated and
48 unsaturated zones in soil must be determined. Several previous studies have
49 attempted to separate SF from SSF, but this topic still needs further investigation
50 (Hursh et al. 1941; Wels et al. 1991; Johst et al. 2013).

51 Harris et al. (1995) proposed a hydrograph separation method for runoff source
52 modeling based on continuous open system isotope mixing, using a variable source
53 area and three isotopic reservoirs. They estimated time-dependent streamflow
54 contributions of SF and SSF in storm rainfall events, and estimated parameters for
55 determining the relationships between saturated area fraction and streamflow, and
56 between saturated area and subsurface water storage (Harris et al. 1995).

57 A stable environmental isotope was used by Tekeli and Sorman (2003) to investigate
58 the rainfall-runoff relationship and to separate SF from SSF in hydrographs, based
59 on analysis of water samples from rainfall, runoff (total discharge), springs
60 (subsurface flows), and wells (groundwater) in the Guvenc Basin, Turkey. Through
61 this approach, they successfully determined the contribution of SSF originating from
62 various sublayers.

63 Foks et al. (2019) used an optimal hydrograph separation technique based on a two-
64 parameter recursive digital filter and specific conductance mass-balance constraints
65 to estimate the base flow contribution to observed flow in river gauges.

66 Some previous studies of SSF at hillslope scale have used existing methods based
67 on the Dupuit-Forchheimer approach, Boussinesq equation, or numerical solution of
68 complex three-dimensional equations (e.g., Troch et al. 1993; Chen et al. 1994a,
69 1994b). Numerical methods give good accuracy, but most hydrologists want simpler
70 methods. Some hydrological models have also been used to estimate SSF (Robinson
71 and Sivapalan 1996; Lee and Chang 2005; Sabzevari et al. 2013; Sabzevari and
72 Noroozpour, 2014).

73 Lee and Chang (2005) developed the geomorphological instantaneous unit
74 hydrograph (GIUH) model for predicting SSF. Surface and subsurface travel time
75 are the most important parameters in the GIUH model. Subsurface travel time is a

76 function of overland length and slope and soil characteristics, e.g., hydraulic
77 conductivity and porosity. Lee and Chang (2005) used the GIUH model to separate
78 SF and SSF in the Heng-Chi basin, Taiwan.

79 Sabzevari et al. (2013) modified the Lee and Chang (2005) model by calculating the
80 SSF hydrograph of the catchment through convoluting the subsurface GIUH model
81 in the infiltration hyetograph. In their modified version, a more accurate saturation
82 model was used to predict SF and SSF according to the Dunne-Black mechanism.
83 Sabzevari et al. (2013) applied the modified model in the Kasilian catchment, Iran,
84 to separate SF and SSF.

85 Sabzevari and Noroozpour (2014) examined the role of hillslope shape and profile
86 curvature on SF and SSF in complex hillslopes and applied a new complex saturation
87 model to separate the saturation region. They used the model to estimate SSF in a
88 small basin, No. 125 in Walnut Gulch, Arizona, USA.

89 The theory of Sabzevari et al. (2013) was used by Petroselli (2020) that generalized
90 the EBA4SUB rainfall-runoff model (Piscopia et al. 2015; Petroselli and Grimaldi
91 2018; Petroselli et al. 2020 a, b), originally developed only for SF estimation,
92 introducing within the model the subsurface flow process and allowing its
93 application to both Hortonian and Dunne-Black runoff formation mechanisms,
94 employing the Width Function Based IUH framework.

95 Laboratory physical models are commonly used to validate the results of SF and SSF
96 estimation models. Essig et al. (2008) devised a laboratory set-up to separate deep
97 flow and surface flow for sloping surfaces. The equipment consisted of a rainfall
98 simulator device with length 1.52 m and width 1.22 m, and a soil box with depth 78
99 cm, which was equipped to measure SSF and the SF separately by two weirs. In
100 Essig et al. (2008), the separation between SF and SSF was also modeled by the

101 Hydrus 2D (numerical) model for different slopes up to 10 degrees, and the results
102 were compared.

103 The runoff coefficient (RC) is used to separate the amount of excess rainfall from
104 infiltration in many hydrological models (e.g. the rational method), in doing so
105 trying to express the relationship between SF and SSF. The RC value indicates the
106 ratio of surface runoff depth to total rainfall depth. Based on RC values, the surface
107 runoff depth and infiltration depth can be determined (Kim and Shin 2018; Kim et
108 al. 2016).

109 RC depends on factors such as soil type and land use, slope and rainfall rate. In this
110 study, we developed a new method for separating SF and SSF in catchments by
111 investigating the effect of slope and rainfall intensity on RC. We verified the method
112 using laboratory data in the hillslope dimension. Finally, we tested the method in
113 separation of SF and SSF for two catchments (Heng-Chi and San-Hsia) in northern
114 Taiwan and compared the modeled results with observed direct runoff.

115 A number of studies have been presented on the separation of surface and subsurface
116 flow from runoff hydrograph(Hursh and Brater, 1941; Wels et al, 1991; Johst et al,
117 2013).

118 Lee et al (2015) introduced a new method to estimate the runoff coefficient through
119 the infiltration analysis based on the comparative results of the existing runoff
120 coefficient method. The effect of rainfall intensity and soil characteristics to runoff
121 coefficient was also analyzed by the FFC-COBRA model and effective rainfall
122 separation method based on NRCS CN. This result showed that runoff coefficient in
123 this study is not only in the range of runoff coefficient, but also over the upper limit
124 of 0.10~0.22 at 'forest, etc' from ASCE.

125 Johst et al (2013) studied in 31 ha headwater basin in Western Germany to separate
126 the surface flow and subsurface flow from runoff hydrograph. In this study, the
127 contribution of infiltration excess and saturation overland flow as well as matrix and
128 preferential flow has been assessed along a deeply incised channel of 300 m length.
129 Measurable parameters and simple algorithms were used to assess the flow rate of
130 the different runoff components. The results showed that during wet conditions the
131 subsurface flow rates exceed the surface flow rates tremendously.

132 The main classification of the sections of this article is as follows: In the first part,
133 the equations of separation of surface and subsurface flow are presented, then the
134 effect of rainfall intensity and slope on surface flow is investigated. In the next
135 section, the results of two laboratory models for measuring surface and subsurface
136 flow are presented and the observed runoff coefficients and the calculated runoff
137 coefficient are evaluated. Finally, the proposed method for two catchments in
138 Taiwan is evaluated.

139 **2. Materials and Methods**

140

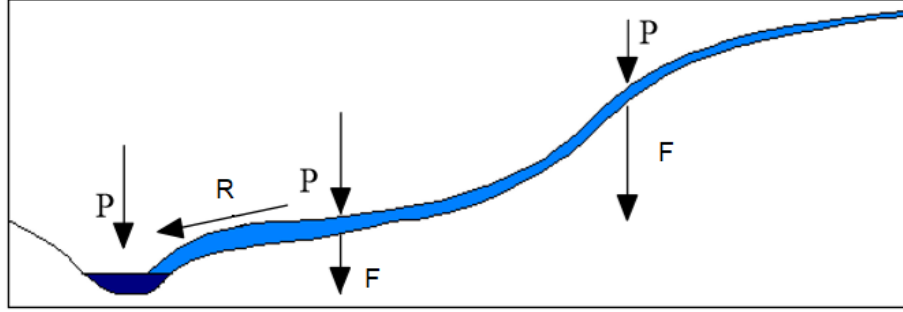
141 **2.1. Separation of surface flow from subsurface flow**

142 The amount of rainfall or liquid precipitation (P) falling on a hillslope (Fig. 1) can
143 be calculated from the sum of surface runoff (R) and infiltration (F):

$$144 \quad P = F + R \quad (1)$$

145 Introducing RC ($R = RC \times P$) and substituting P with R/RC in Eq. 1, we can calculate
146 the ratio of surface runoff depth to infiltration (subsurface runoff) depth as a function
147 of RC :

$$148 \quad R/F = RC/(1-RC) \quad (2)$$



149

150 Fig. 1: Schematic diagram of the rainfall-runoff process in a hillslope, where P is precipitation, F
 151 is infiltration, and R is surface runoff (Tarboton, 2003)

152

153 In this study, we assumed that the bedrock is close to the surface and that all
 154 infiltrated water is SSF and does not contribute to groundwater. In the steady state
 155 condition with excess rainfall intensity (I_e) on a hillslope, the maximum surface and
 156 subsurface flow (Q_s and Q_{sub} , respectively) can be calculated as (Akan and
 157 Houghtalen 2003):

158
$$Q_s = I_e \times A \quad (3)$$

159 and

160
$$Q_{sub} = I_f \times A \quad (4)$$

161 where I_f is the recharge rate into the soil layer and A is the contributing area of the
 162 hillslope. The ratio (m) of the SF peak to the SSF peak can be calculated as:

163
$$m = \frac{Q_s}{Q_{sub}} = \frac{I_e \times A}{I_f \times A} = \frac{I_e}{I_f} \quad (5)$$

164 or:

165
$$m = \frac{I_e}{I_f} = \frac{R}{F} \quad (6)$$

166 where R is surface runoff depth and F is infiltration depth. From Eq. 2, we have ratio
 167 of the SF peak to the subsurface flow peak as a function of RC, so:

168
$$m = \frac{Q_s}{Q_{sub}} = \frac{RC}{(1-RC)} \quad (7)$$

169 Based on Eq. 3, we can calculate the coefficients m and RC if we know peak
170 discharge as SSF and SF. In the next step, we need to validate Eq. 3 to investigate
171 the relationship between RC and SF and SSF.

172 Assuming that base flow is zero ($Q = Q_s + Q_{sub}$), based on total observed flow (direct
173 runoff) Q_s and Q_{sub} are calculated as follows:

174
$$Q_s = RC \times Q$$

175
$$Q_{sub} = (1-RC) \times Q \quad (8)$$

176 Thus using Eq. 8, SF and SSF can be calculated separately. In this study, the results
177 obtained using Eq. 8 were validated using the results of laboratory rain simulations
178 on artificial slopes.

179 The most important innovation of this study is that the separation of surface flow
180 from subsurface flow according to Eq. 8 based on runoff coefficient. RC was
181 calculated only from the observed surface flow. In this research, two laboratory
182 models and observed subsurface flow and observed surface flow were used to
183 evaluate the Eq.8.

184 **2.2. Calculation of runoff coefficient (RC)**

185 . Runoff coefficient is the percentage of rainfall that is converted to runoff.
186 Calculation of RC is complex due to the heterogeneity of infiltration across
187 catchments, and in practice it is impossible to provide an average RC for a
188 catchment. For small hillslopes, we can calculate the average RC by measuring total
189 runoff from the hillslope, using one of the following two methods:

190 Method 1) RC is calculated as:

191
$$RC = V / (P \times A) \quad (9)$$

192 where V is runoff volume (i.e. the area below the graph of surface runoff hydrograph)
193 and P is rainfall depth. This method is more accurate than method 2.

194 Method 2) The RC value is obtained by the rational method, used to predict the
195 runoff peak of small basins, and it is calculated as:

$$196 \quad RC = Q_p / (0.278 \times i \times A) \quad (10)$$

197 where Q_p is peak surface runoff ($\text{m}^3 \text{s}^{-1}$), i is rainfall intensity (mm h^{-1}), and A is
198 basin area (km^2).

199 **2.2.1. Relationship between rainfall and RC**

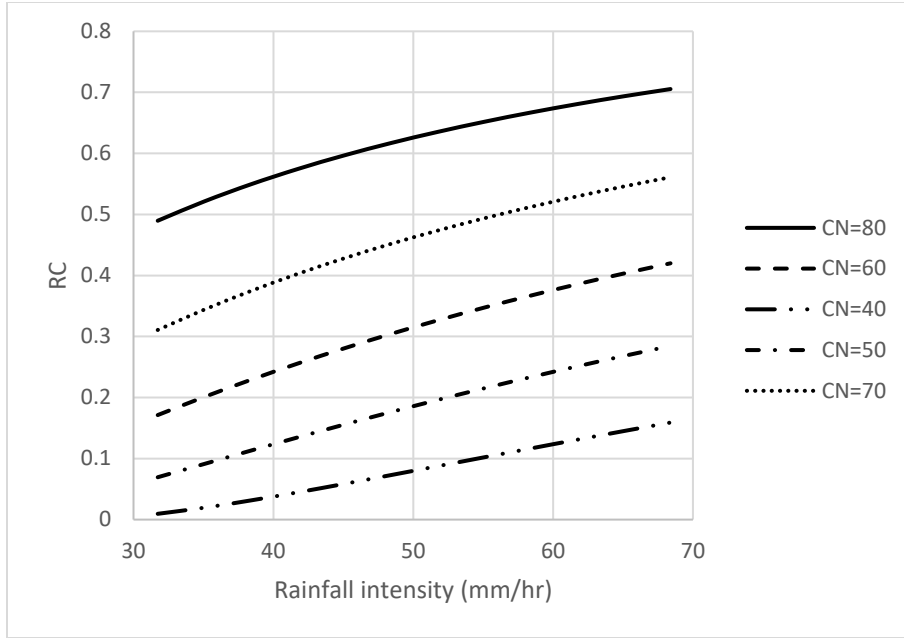
200 In general, greater amounts of rainfall and lower infiltration rates lead to higher
201 surface runoff or higher RC values.

202 The SCS-CN infiltration method calculates RC ($= R/P$) using the following equation
203 (Mishra and Singh 2013):

$$204 \quad RC = R/P = [(P - 0.2 \times S)^2 / (P \times (P + 0.8 \times S))] \quad (11)$$

205 where P is rainfall depth in inches and S is potential maximum retention, which is
206 equal to $(1000/\text{CN} - 10)$, where CN is the selected curve number based on land use,
207 group (from A, sand, to D, clay) and antecedent moisture conditions (from I, dry
208 soil, to III, wet soil) (Chow et al. 1962).

209 Figure 2 shows the change in RC as a function of change in rainfall intensity from
210 31.73 to 63.46 mm h^{-1} for a 3-hour rainfall event for different values of CN based on
211 Eq. (11).



212

213 Fig. 2: Relationship between rainfall intensity and RC for different CN values.

214

215 The CN range for soils with high, medium, and low permeability is 10-30, 40-60,
 216 and 70-90, respectively, which directly influences RC. For example, a 20 mm
 217 increase in rainfall leads to an increase of around 25%, 15%, and 3% in RC for high,
 218 medium, and low permeability soils, respectively.

219 **2.2.2. Effect of slope on RC**

220 Slope is another influential parameter on surface runoff and infiltration (Ribolzi et
 221 al. 2011; Morbidelli et al. 2015; Morbidelli et al. 2018). In general, with steeper
 222 ground slope, the potential for infiltration is lower and consequently the amount of
 223 surface runoff generated will be higher (RC increase).

224

226 Table 1 presents the RC values for different types of soils and land uses on different
 227 slopes (Liu and De Smedt, 2004).

228 The runoff coefficient for different slopes can be calculated as (Liu and De Smedt,
 229 2004):

230
$$C = C_0 + (I - C_0) \times (S / (S + S_0)) \quad (12)$$

231 where C is RC for slope S % and C_0 is RC for horizontal slope S_0 (0%), which is
 232 calculated from Table 2.

233

234 Table 1. Effect of slope and land use on RC

235 (Liu and De Smedt, 2004)

Land use	Slope (%)	Sand	Loamy sand	Sandy loam	Loam	Silt loam	Silt	Sandy clay loam	Clay loam	Silty clay loam	Silty clay	Clay
Forest	<0.5	0.03	0.07	0.10	0.13	0.17	0.20	0.23	0.27	0.33	0.37	0.40
	0.5-5	0.07	0.11	0.14	0.17	0.21	0.24	0.27	0.31	0.37	0.41	0.44
	5-10	0.13	0.17	0.20	0.23	0.27	0.30	0.33	0.37	0.43	0.47	0.50
	>10	0.25	0.29	0.32	0.35	0.39	0.42	0.45	0.49	0.55	0.59	0.62
Grass	<0.5	0.13	0.17	0.20	0.23	0.27	0.30	0.33	0.37	0.43	0.47	0.50
	0.5-5	0.17	0.21	0.24	0.27	0.31	0.34	0.37	0.41	0.47	0.51	0.54
	5-10	0.23	0.27	0.30	0.33	0.37	0.40	0.43	0.47	0.53	0.57	0.60
	>10	0.35	0.39	0.42	0.45	0.49	0.52	0.55	0.59	0.65	0.69	0.72
Crop	<0.5	0.23	0.27	0.30	0.33	0.37	0.40	0.43	0.47	0.53	0.57	0.60
	0.5-5	0.27	0.31	0.34	0.37	0.41	0.44	0.47	0.51	0.57	0.61	0.64
	5-10	0.33	0.37	0.40	0.43	0.47	0.50	0.53	0.57	0.63	0.67	0.70
	>10	0.45	0.49	0.52	0.55	0.59	0.62	0.65	0.69	0.75	0.79	0.82
Bare Soil	<0.5	0.33	0.37	0.40	0.43	0.47	0.50	0.53	0.57	0.63	0.67	0.70
	0.5-5	0.37	0.41	0.44	0.47	0.51	0.54	0.57	0.61	0.67	0.71	0.74
	5-10	0.43	0.47	0.50	0.53	0.57	0.60	0.63	0.67	0.73	0.77	0.80
	>10	0.55	0.59	0.62	0.65	0.69	0.72	0.75	0.79	0.85	0.89	0.92

236

237 Table 2. RC values for different land uses and soil types on land with zero slope (source: Liu and
 238 De Smedt, 2004)

Land use	Sand	Loamy sand	Sandy loam	Loam	Silt loam	Silt	Sandy clay loam	clay loam	Silty clay loam	Sandy clay	Silty clay	Clay
Forest	0.680	0.650	0.620	0.590	0.560	0.530	0.500	0.470	0.440	0.410	0.380	0.350
Grass	0.580	0.551	0.522	0.493	0.464	0.435	0.405	0.376	0.347	0.318	0.289	0.260
Crop	0.500	0.471	0.442	0.413	0.384	0.355	0.325	0.296	0.267	0.238	0.209	0.180
Bare soil	0.420	0.393	0.365	0.338	0.311	0.284	0.256	0.229	0.202	0.175	0.147	0.120

239

240 3. Physical model description

241 Laboratory tests were conducted using an experimental set-up at the Hydraulic
 242 Laboratory of the Civil Engineering Department at Estahban Azad University, Iran
 243 (Fig. 3). It consists of a rainfall simulator over a soil box (length 1.92 m, width 1 m,
 244 depth 35 cm, which was filled with loamy sand soil and sandy clay soil. Tests were

245 run with four slopes (0, 3, 6, and 9 degrees) and three rainfall intensities (31.73, 47.6,
246 and 63.46 mm/ h). The rainfall duration in most event has been about 300 minutes.
247 Each test has been tested after drying the soil that soil moisture error does not affect
248 measurements. The intensity of rainfall was tested by nozzles before each test.
249 SF and SSF were measured by two separate weirs.

250



251

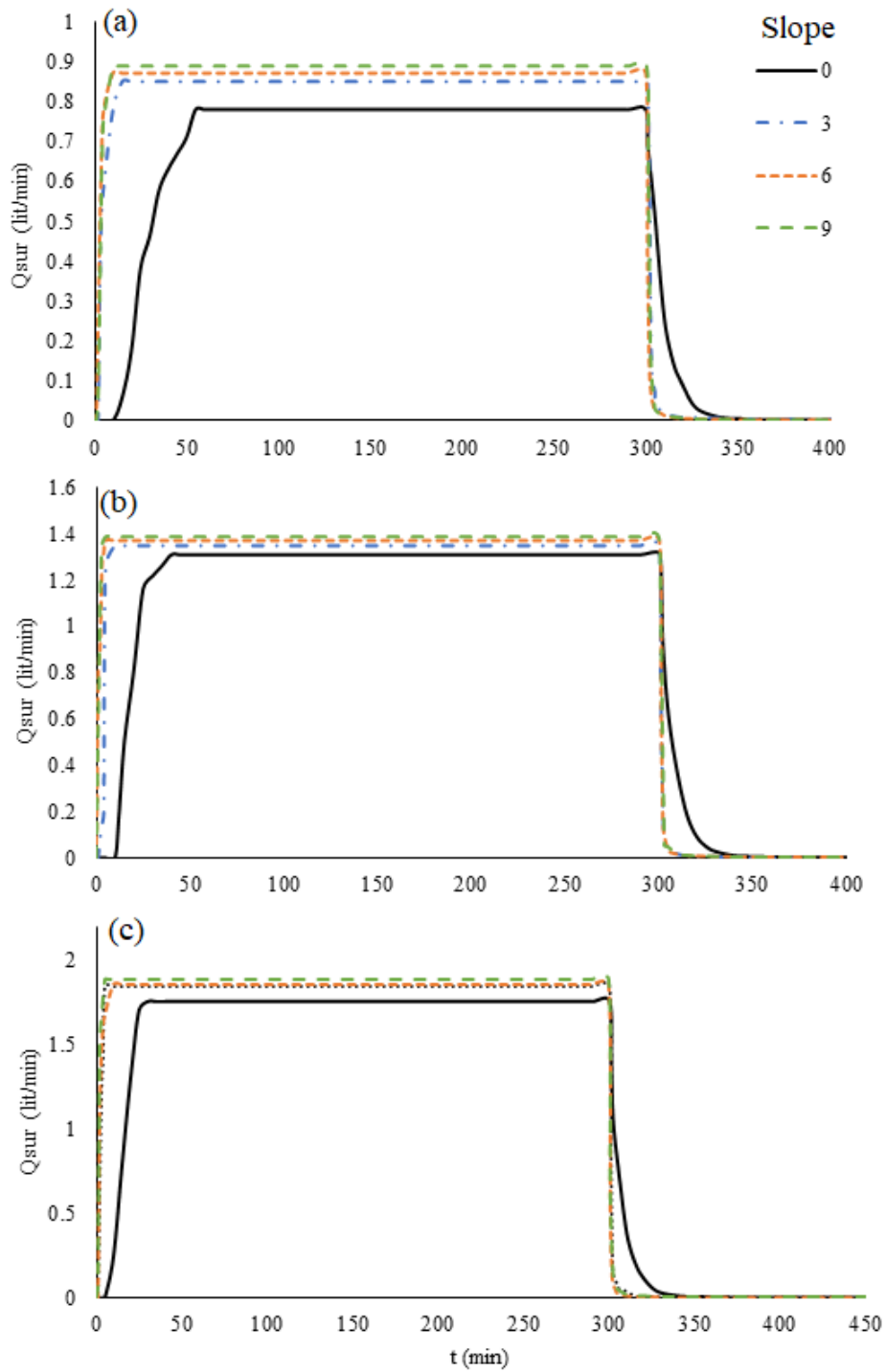
252 Fig. 3. Physical soil model and rainfall simulator used in laboratory tests.

253

254 **4. Results and Discussion**

255 **4.1 Hydrograph produced by the physical model**

256 For loamy sand soil, the maximum SF measured at the outlet of the physical model
257 varied between 0.78-0.89, 1.31-1.39, and 1.76-1.89 $l\ min^{-1}$ for the 31.73, 47.6, and
258 63.46 $mm\ h^{-1}$ rainfall events, respectively (Figs. 4a-4c). The maximum SSF ranged
259 between 0.112 and 0.228 $l\ min^{-1}$ (Table 3). Substituting the maximum values of
260 observed SF and SSF into Eq. 7 allowed us to calculate RC of the loamy sand (Table
261 3) for different rainfall events and slopes (Table 4). The observed and calculated
262 runoff coefficient showed a significant positive correlation ($R^2 = 0.93$) (Fig. 5a).

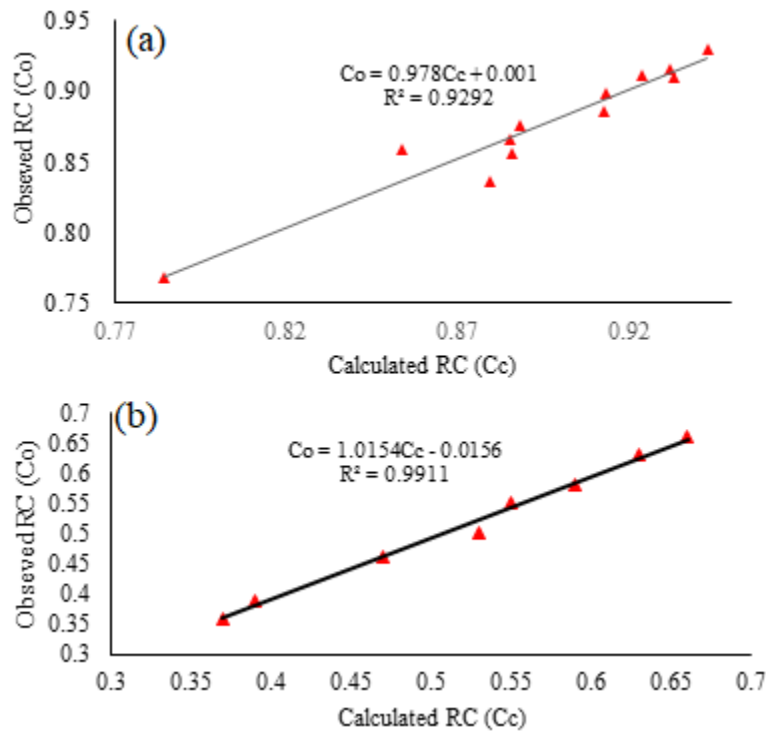


264

265 Fig. 4. Observed SF from the physical model with loamy sand soil with different land slope (0-9
266 degrees) at rainfall intensity of a) 31.73 mm h⁻¹, b) 47.6 mm h⁻¹, and c) 63.46 mm h⁻¹.

267

268 Table 3 shows the maximum values of SF and SSF, SF to SSF ratio, calculated RC
 269 (Cc) and observed RC (Co) according to the surface runoff volume method.



270
 271 Fig. 5. Correlation between calculated and observed RC for a) loamy sand and b) sandy clay soil.

272
 273 Table 3. Observed and calculated value of RC based on observations of SF and SSF obtained in a
 274 physical model with loamy sand and sandy clay soil.

275

Type of soil	Rainfall intensity mm h ⁻¹	Slope, degrees	SSF max. l min ⁻¹	SF max. l min ⁻¹	SF/SSF	Calculated RC Eq. 7 (C _c)	Observed RC Eq. 9 (C _o)
Loamy sand	31.73	0	0.214	0.78	3.64	0.784	0.768
		3	0.116	0.85	7.33	0.880	0.836
		6	0.112	0.87	7.77	0.886	0.856
		9	0.112	0.89	7.95	0.888	0.876
Loamy sand	47.6	0	0.224	1.31	5.85	0.854	0.859
		3	0.129	1.35	10.47	0.913	0.886
		6	0.130	1.37	10.54	0.913	0.899
		9	0.114	1.39	12.19	0.924	0.912
Loamy sand	63.46	0	0.228	1.76	7.72	0.885	0.866
		3	0.132	1.85	14.02	0.933	0.910
		6	0.135	1.86	13.78	0.932	0.915
		9	0.114	1.89	16.58	0.943	0.930
		0	0.500	0.00	0.00	-	-

Sandy clay	31.73	3	0.500	0.00	0.00	0.00	0.00
		6	0.320	0.18	0.56	0.36	0.36
		9	0.270	0.23	0.85	0.46	0.46
		0	1.00	0.00	0.00	-	-
Sandy clay	47.6	3	0.60	0.40	0.67	0.40	0.39
		6	0.47	0.53	1.13	0.53	0.50
		9	0.45	0.55	1.22	0.55	0.55
		0	1.50	0.00	0.00	-	-
Sandy clay	63.46	3	0.62	0.88	1.42	0.59	0.58
		6	0.55	0.95	1.73	0.63	0.63
		9	0.50	1.00	2.00	0.67	0.66

276

277 In tests with loamy sandy soil, the observed RC initially increased with increasing
278 slope, e.g. at a slope of 3 degrees above the horizontal (0 degrees), it increased by
279 about 12% on average (Table 3). However, a further increase in slope from 3 to 6
280 degrees and from 6 to 9 degrees gave little change in RC. The average increase in
281 SF with an increase in rainfall intensity from 31.73 mm h⁻¹ to 47.6 and 63.46 mm⁻¹
282 was between 6.5 and 8.5%. In our results, the RC depended on soil type, slope, and
283 land use, and was weakly related to rainfall intensity in different events. Thus in
284 practice, it was impossible to calculate RC accurately.

285 The observed data for sandy clay soil were similar to those for loamy sand soil (Table
286 3 and Fig. 5b). The calculated and observed RC values for the sandy clay were lower
287 than those for the loamy sand, because of the higher permeability of the sandy clay.
288 At 0 degrees of slope, all rainfall contributed to subsurface flow for the sandy clay,
289 and thus the RC is not shown in Table 3. At 6 degrees of slope, the RC increased by
290 28% and 8% for a rainfall intensity of 47.6 and 63.4 mm h⁻¹, respectively (Table 3).
291 Increasing the rainfall intensity also led to increasing RC for the sandy clay, for
292 instance for a slope of 6 degrees, the RC for a rain intensity of 31.7, 47.6, and 63.46
293 mm h⁻¹ was 0.36, 0.53, and 0.59, respectively (Table 4).

294 The results of tests in the physical model for two different soils clearly confirmed
 295 that the method developed in this study can be recommended as suitable and simple
 296 approach to separate SF and SSF in rainfall-runoff analysis of hillslopes. As shown,
 297 different parameters, e.g., soil type, land use, slope, and rainfall intensity, influenced
 298 the RC value.

299 **4.2. Verification based on observed and calculated SSF and SF**

300 In this section, for more accurate validation of the proposed method, surface and
 301 subsurface flow information of the other two different soils were used. The first soil
 302 was clay loam and this soil was evaluated by the device according to Figure 3. The
 303 second soil was loamy and SF and SSF information was examined based on
 304 Morbidelli et al. (2015) study.

305 For first verification of the method, we compared the observed and calculated SSF
 306 and SF values obtained for different rainfall rates and slopes (Table 4). For this, we
 307 filled the soil box in the physical model (Fig. 3) with a clay loam soil and applied
 308 three different rainfall intensities (15.63, 31.3, and 46.9 mm/h). For this experiment,
 309 the RC for a slope of 3, 5, and 10 degrees was 0.61, 0.67, and 0.79, respectively.

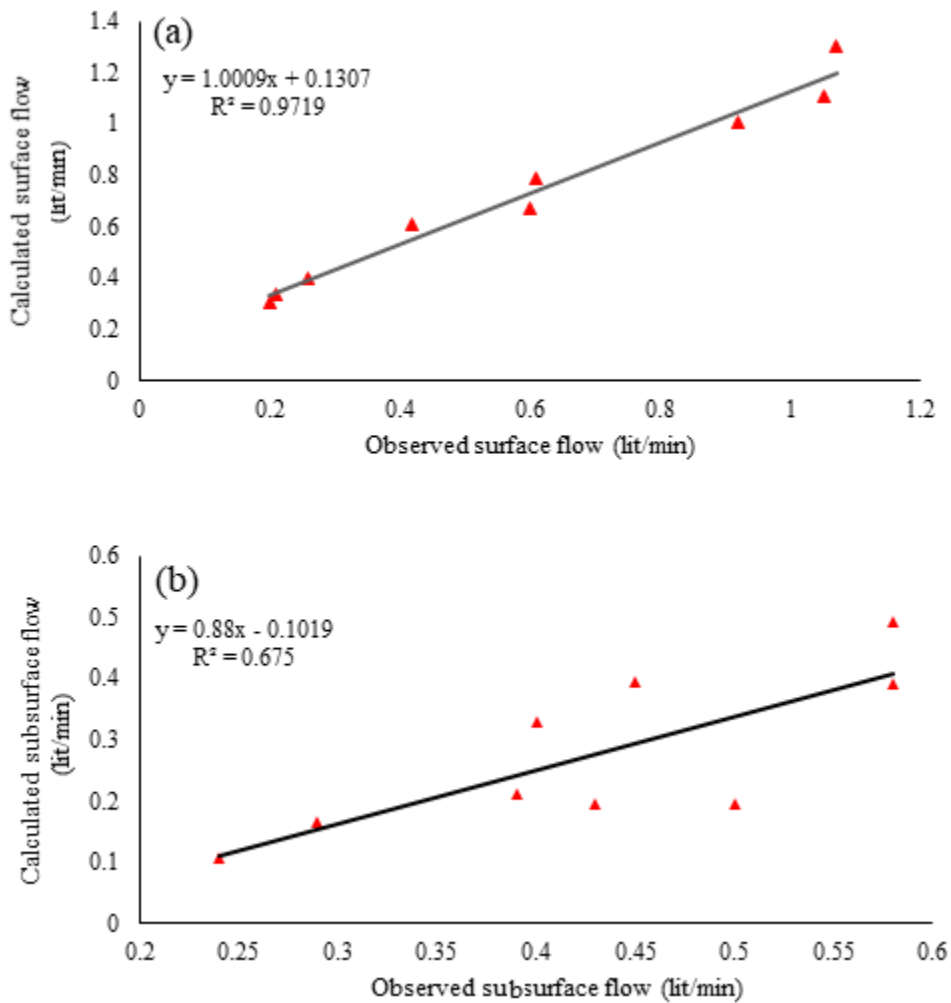
310 Table 4. Observed and calculated SSF and SF for a clay loam soil

311 SF(PE) is SF peak error, SFF(PE) is SFF peak error

Rainfall mmhr ⁻¹	Slope Degrees	Observed (l min ⁻¹)		Calculated (l min ⁻¹)		SF(PE)	SFF(PE)
		SSF	SF	SSF	SF		
15.63	3	0.5	0.200	0.195	0.305	0.53	0.61
15.63	6	0.29	0.210	0.165	0.335	0.60	0.43
15.63	9	0.24	0.259	0.105	0.395	0.53	0.56
31.3	3	0.58	0.420	0.390	0.610	0.45	0.33
31.3	6	0.4	0.600	0.330	0.670	0.12	0.18
31.3	9	0.39	0.610	0.210	0.790	0.30	0.46
46.9	3	0.58	0.920	0.490	1.000	0.09	0.16
46.9	6	0.45	1.050	0.390	1.110	0.06	0.13
46.9	9	0.43	1.070	0.190	1.300	0.21	0.56

312

313 Figure 6 illustrates the estimated versus observed SF and SSF values. The correlation
314 coefficient of predicted SF in this experiment was 0.972, which is good, and the
315 correlation coefficient of predicted SSF was 0.675, which is acceptable.



316
317 Fig. 6. Correlation between a) observed and calculated SSF and b) observed and calculated SF
318 for a clay loam soil.

319
320 Surface flow measurement is recorded more accurately in laboratory models, but
321 there is more error in measuring subsurface flow due to soil moisture storage and the
322 influence of other factors, and this has reduced the correlation coefficient in
323 subsurface flow.

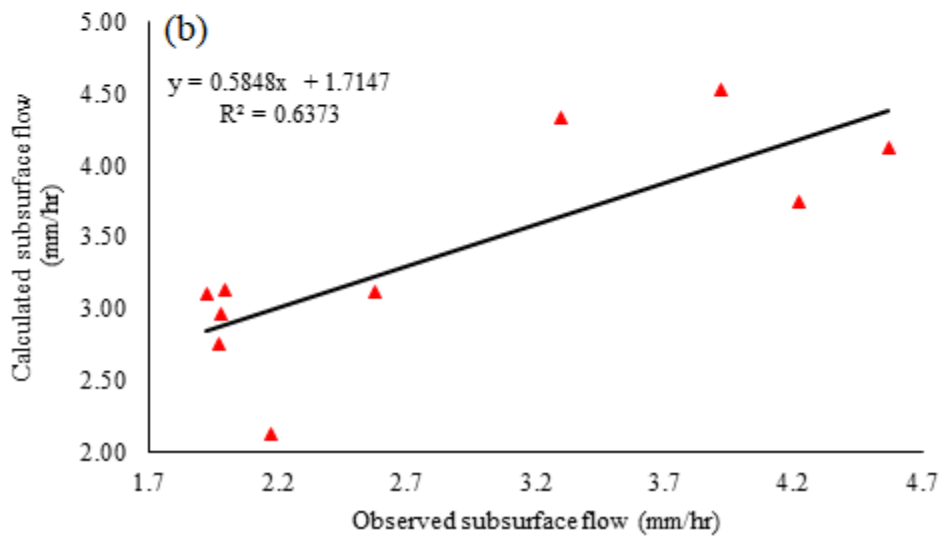
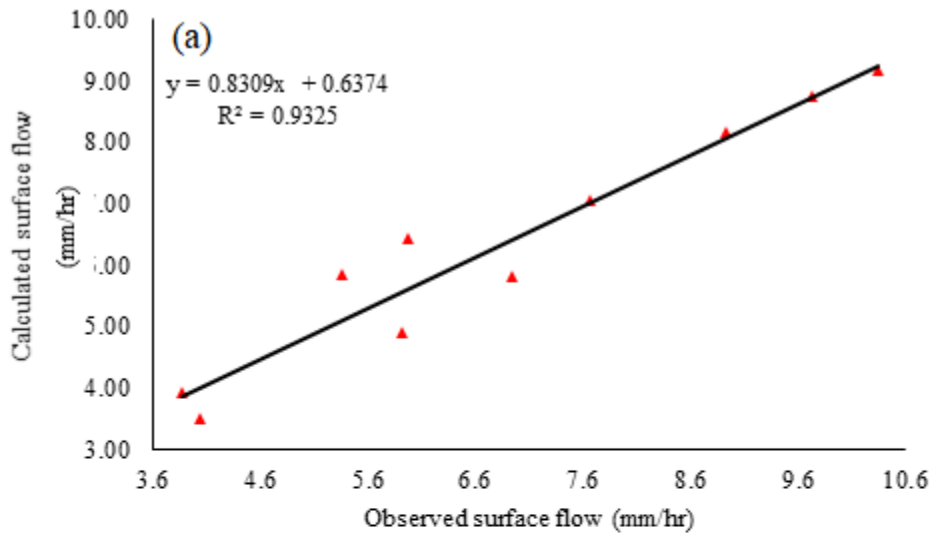
324 Moving from laboratory scale to real catchment scale, usually the lack of observed
325 SSF data is the main obstacle to validating SSF forecasting models. Available SSF
326 data in the hillslope dimension are generally used to validate models (Tiefan et al.
327 2005; Brown et al. 1999; Ameli et al. 2015; Fariborzi et al. 2019). For a more
328 accurate validation of the method proposed in this study, rainfall simulator data
329 reported by Morbidelli et al. (2015) were used (Table 5). Their data were obtained
330 used a soil box measuring $152 \times 122 \times 78$ cm in length, width, and thickness,
331 respectively, and containing loamy soil. The slope of the box was adjustable from 0
332 to 10 degrees. Table 5 shows the observed SF and SSF values for different rainfall
333 rates and two slopes, 5 and 10 degrees. For instance, the calibrated values for RC
334 were 0.53 and 0.65 for slopes of 5 and 10 degrees respectively. The SF and SSF
335 values were also calculated using our method (Eq. 8) (Table 6) and the results were
336 compared with observed maximum SF and SFF reported by Morbidelli et al. (2015).
337 The correlation coefficient of SF prediction values in this case was 0.93, which is a
338 very good value, and that of SFF prediction values was 0.64, which is acceptable
339 (Fig. 7).

340
341 Table 5. Observed and calculated surface flow (SF) and subsurface flow (SSF) (observed) in tests
342 in a physical model (data from Morbidelli et al. 2015)

343 SF(PE) is SF peak error, SFF(PE) is SFF peak error

Slope (degrees)	Total flow (mm h ⁻¹)	Observed SF (mm h ⁻¹)	Observed SSF (mm h ⁻¹)	Calculated SF (mm h ⁻¹)	Calculated SSF (mm h ⁻¹)	SF(PE)	SFF(PE)
5	6.62	4.04	2.58	3.97	2.65	0.02	0.03
5	9.22	5.92	3.3	4.89	4.33	0.17	0.31
5	9.59	5.37	4.22	5.75	3.84	0.07	0.09
5	10.55	5.98	4.57	5.59	4.96	0.07	0.09
5	11.59	7.67	3.92	6.76	4.83	0.12	0.23
10	6.05	3.88	2.17	3.93	2.12	0.01	0.02
10	8.93	6.94	1.99	5.80	3.13	0.16	0.57
10	10.9	8.93	1.97	8.72	2.18	0.02	0.11
10	12.26	10.34	1.92	9.81	2.45	0.05	0.28

345



346

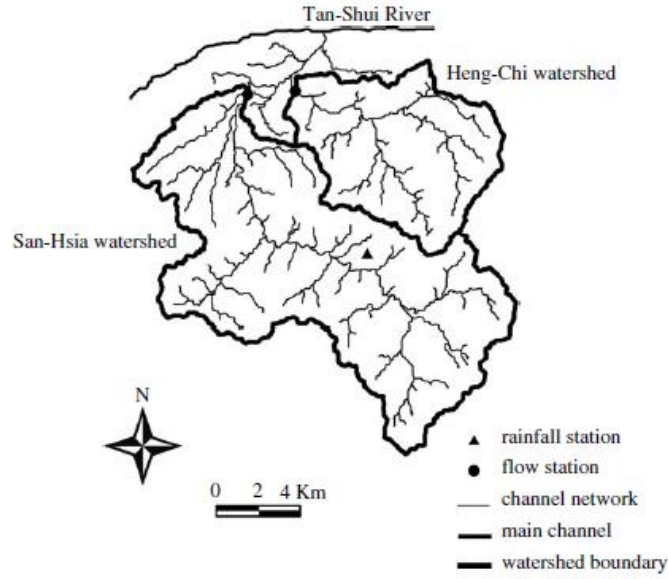
347 Fig. 7. Correlation between a) observed and calculated surface flow and b) observed and calculated
348 surface flow for clay loam soil, based on data in Morbidelli et al. (2015).

349

350 The results showed that the correlation coefficient for predicted SF in this
351 experiment was greater than 0.97, which is very good, and that for predicted SSF
352 was 0.635, which is acceptable.

353 **4.3 Predicting the SF and SSF hydrograph at catchment scale**

354 Separation of SF hydrograph and SSF hydrograph from observed flood hydrograph
355 is very important for hydrologists. In the previous sections, we focused on the
356 separation of SF and SF peaks of hillslopes in the laboratory, but in this section, the
357 proposed RC method was applied to evaluate the separation method in the catchment
358 scale. For further model verification, data on peak SF and SSF from the Heng-Chi
359 and San-Hsia catchments in northern Taiwan were used (Fig. 8 and Table 6). The
360 Heng-Chi catchment ranges in elevation from 20 m at the outlet to 970 m, and
361 occupies an area of 53.23 km², which is covered by forest (70%), cultivated land
362 (25%), and urban area (5%). The San-Hsia catchment is similar, with elevation
363 ranging between 30 and 1770 m and area 125.88 km², with 75% forest, 20%
364 cultivated land, and 5% urban land use.



365

366 Fig. 8. Location of the Heng-Chi and San-Hsia catchments in Taiwan (after Chang and Lee 2008).

367 **4.3.1. Subsurface GIUH model**

368 Chang and Lee (2005) revised the GIUH model to estimate SSF in catchments. In
 369 this model, the Darcy's law was adopted to estimate the runoff travel time in
 370 subsurface-flow regions. Based on the Horton-Strahler ordering law, any catchment
 371 of order Ω can be divided into a series of runoff states. The catchment hydrologic
 372 response can be considered to be functions of the runoff path probabilities and runoff
 373 travel time probabilities in different runoff states (Rodriguez-Iturbe and Valdes,
 374 1979).

375 Let x_{o_i} denotes the i th-order overland-flow regions in catchment, denotes the x_{sub_i}
 376 i th-order subsurface-flow regions, and x_i denotes the i th-order channels, in which
 377 $i = 1, 2, \dots, \Omega$. Ω is maximum order of catchment. The subsurface IUH can be
 378 expressed analytically by (Lee and Chang, 2005):

379
$$u_{sub}(t) = \sum_{w_{sub} \in W_{sub}} [f_{x_{sub}}(t) * f_{x_i}(t) * f_{x_j}(t) * \dots * f_{x_{\Omega}}(t)]_{w_{sub}} P(w_{sub}) \quad (13)$$

380 where $u_{sub}(t)$ is subsurface-flow IUH, w_{sub} is the subsurface flow path space given as
 381 $W_{sub} = \langle x_{sub_1}, x_i, x_j, \dots, x_{\Omega} \rangle$, $P(w_{sub})$ are the probabilities of a raindrop adopting a subsurface
 382 flow path of w_{sub} .

383 In this study, the subsurface GIUH values for these two case study catchments were
 384 compared with results obtained using the RC-based model developed in this study.

385
 386
 387
 388
 389
 390
 391
 392
 393
 394
 395

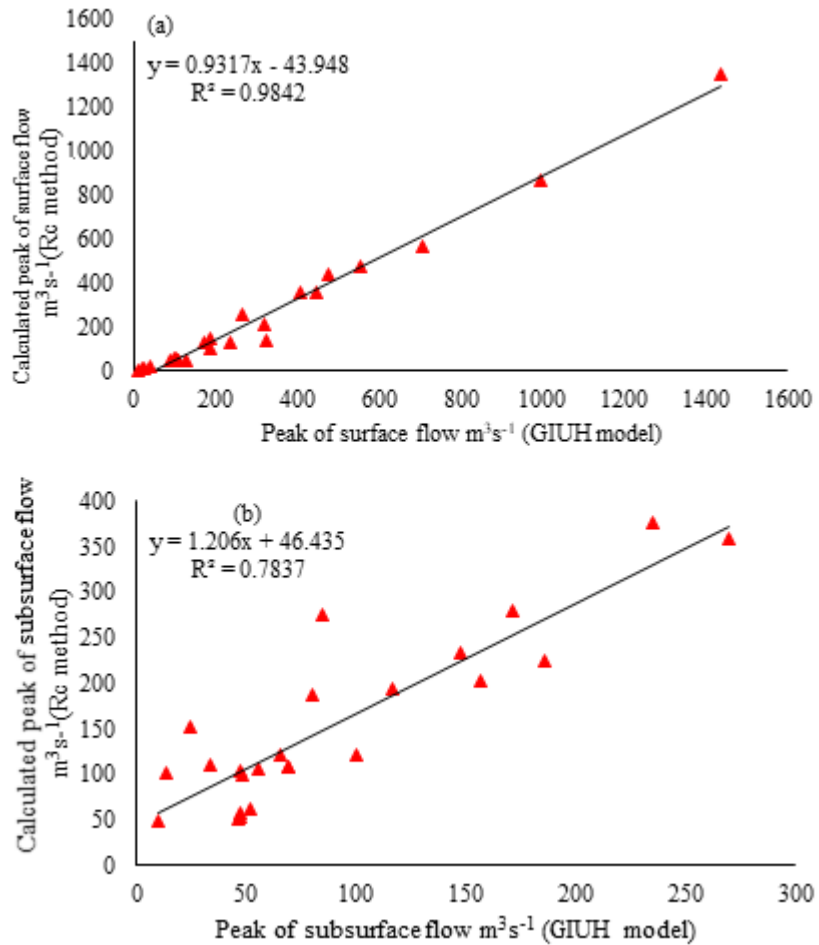
396 Table 6. Recorded SF, peak SF and SSF estimates obtained using the GIUH method, for the Heng-
 397 Chi and San-Hsia catchments in northern Taiwan (source: Chang and Lee 2008)

Catchment	Event date	DRH (GIUH method)		SF (GIUH method)		SSF (GIUH method)	
		Q_p (m^3s^{-1})	T_p (hr)	Q_p (m^3s^{-1})	T_p (hr)	Q_p (m^3s^{-1})	T_p (hr)
Heng-Chi	08/16/1984	157.8	67	88.8	66	69.3	68
	09/16/1985	587.7	8	553.7	7	34.3	9
	09/17/1986	455.9	41	407.9	40	48.2	43
	07/27/1987	161.5	7	105.5	7	55.9	8
	09/08/1987	318.0	36	238	36	80.0	37
	08/18/1990	486.4	32	476.4	31	10.1	32
	06/05/1993	173.4	11	107	11	66.3	12
	07/10/1994	57.0	12	11	11	45.9	12
	07/30/1996	242.1	30	173	29	68.6	34
	06/22/1997	70.6	5	24	6	47.2	7
	06/18/1999	153.6	4	107	4	47.1	5
	08/22/2000	72.5	18	21	18	52.1	20
	10/31/2000	309.8	18	263	17	46.5	24
San-Hsia	06/03/1983	243.6	14	127	14	116.5	15

09/16/1985	1449.1	8	1435	8	13.4	9
07/14/1987	142.1	12	42	11	99.6	15
07/27/1987	336.5	8	189	8	148.0	9
08/18/1990	1022.1	31	997	31	25.1	31
08/30/1990	941.8	16	707	15	234.7	16
09/07/1990	410.0	25	325	25	85.2	26
07/10/1994	255.8	13	99	12	156.7	13
10/09/1994	487.8	20	318	20	170.7	24
07/30/1996	717.0	31	447	30	270.1	34
08/17/1997	374.6	32	189	32	185.7	34

398

399 In Figure 9a, the SF values for the catchments calculated using Eq. 8 are compared
400 with the values obtained by the GIUH method in the two catchments recorded by
401 Chang and Lee (2008) (column 3, Table 6). The correlation coefficient was 0.98,
402 which is very good. Figure 9b also shows the SSF values for the two catchments
403 calculated using Eq. 8 and those estimated by the GIUH model. The correlation
404 coefficient in this case was lower, 0.78.



405

406

407 Fig. 9. Comparison of a) peak SF and b) peak SFF in Heng-Chi and San-Hsia catchments
 408 calculated by the RC method developed in this study and by Chang and Lee (2008) using the GIUH
 409 model.

410 Furthermore, the SSF and SF hydrographs for Heng-Chi (July 1996) and San-Hsia
 411 (August 1997) calculated using the GIUH model were compared with those
 412 produced using the RC method (Fig. 10). To evaluate model fitness for this purpose,
 413 coefficient of efficiency (CE) and relative error in peak (REP) were calculated
 414 (Chang and Lee 2008):

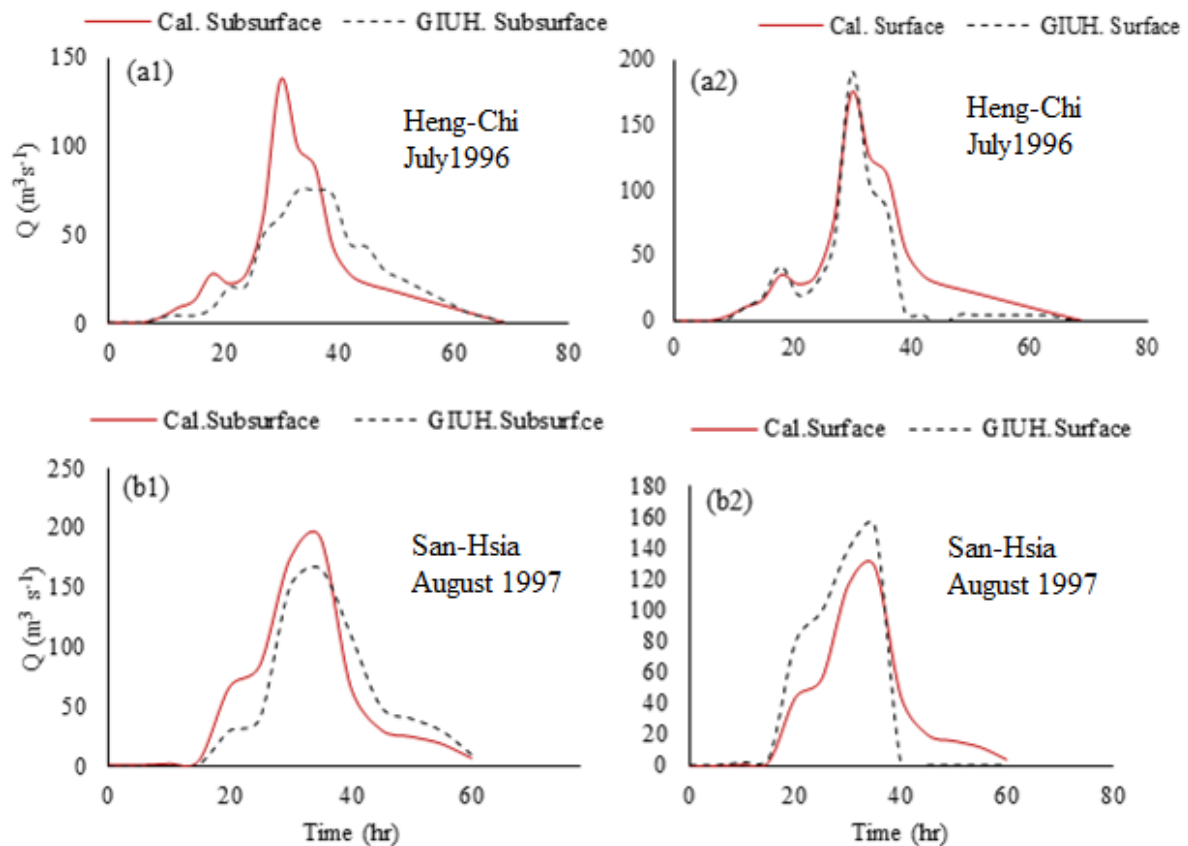
415
$$CE = 1 - \frac{\sum_{t=1}^n [Q_o - Q_s]^2}{\sum_{t=1}^n [Q_o - \bar{Q}_o]^2} \quad (14)$$

416
$$REP = 100 \times [Q_{p_s} - Q_{p_o}] / Q_{p_o} \quad (15)$$

417

418 where Q_o is observed discharge at time t ; Q_s is simulated discharge at time t ; \bar{Q}_o is
 419 average observed discharge during a storm event; n is number of discharge records
 420 during the storm event; Q_{p_s} is peak discharge of the simulated hydrograph; and Q_{p_o}
 421 is observed peak discharge.

422 The value of CE is between 0 and 1 and CE values above 0.8 are acceptable. The
 423 CE was found to be 0.8 and 0.81 for SF, and 0.7 and 0.81 for SSF, in the Heng-Chi
 424 and San-Hsia catchment, respectively. Peak error in Heng-Chi was 8% and 80% for
 425 SF and SSF, respectively, while it was %18 and %17, respectively, in San-Hsia
 426 catchment. Thus, peak error in SSF in Heng-Chi was unacceptably large.



427

428 Fig. 10. Hydrographs calculated by the RC method and simulated by the GIUH model for: 1) SF
 429 and 2) SSF in a) Heng-Chi catchment, July 1996 and b) San-Hsia catchment, August 1997.

430 **5. Conclusions**

431 Separation of surface runoff and subsurface runoff from observed data in catchments
 432 is difficult, due to the hydrological complexities of runoff. In many permeable
 433 catchments with high vegetation cover, subsurface runoff is of great importance. In
 434 this study, we applied the concept of runoff coefficient (RC) to devise a simple and
 435 practical method for separating surface and subsurface flow in direct runoff from
 436 hillslopes or catchments. The accuracy of the method is directly dependent on the
 437 accuracy of RC values. We investigated the effect of slope, rainfall intensity, and
 438 soil type on RC. Using the SCS-CN infiltration method, we also tested the effect of
 439 rainfall intensity on RC for soils with different curve number.

440 To verify the method, the results were compared with those of laboratory tests on
441 different soils using a rainfall simulator and an adjustable soil box, and with values
442 predicted by the geomorphological instantaneous unit hydrograph (GIUH) model for
443 two watersheds, Heng-Chi and San-Hsia, in Taiwan. Comparison with laboratory
444 values revealed that our RC-based method accurately predicted peak surface flow
445 and subsurface flow in different soils, with correlation coefficient (CE) 0.93 and
446 0.65, respectively. Comparison with surface and subsurface runoff hydrographs for
447 Heng-Chi and San-Hsia catchments, obtained using the GIUH model. Based on
448 results, the CE was found to be 0.8 and 0.81 for SF, and 0.7 and 0.81 for SSF, in the
449 Heng-Chi and San-Hsia catchment, respectively. Peak error in Heng-Chi was 8%
450 and 80% for SF and SSF, respectively, while it was %18 and %17, respectively, in
451 San-Hsia catchment. Thus, peak error in SSF in Heng-Chi was unacceptably large.
452 Thus if RC can be calculated accurately, our method can successfully separate
453 surface and subsurface flow in total runoff.

454 **10. Acknowledgements**

455 This article is based on data in a PhD thesis in Water and Hydraulic Structures (Amin
456 Afshar Ardekani) at Islamic Azad University, Estahban Branch, Fars, Iran.

457

458 **11. References**

459 Akan, A. O., & Houghtalen, R. J. (2003). Urban hydrology, hydraulics, and stormwater quality:
460 engineering applications and computer modeling. John Wiley & Sons.

461 Ameli, A. A., Craig, J. R., & McDonnell, J. J. (2015). Are all runoff processes the same? Numerical
462 experiments comparing a Darcy-R ichards solver to an overland flow-based approach for
463 subsurface storm runoff simulation. *Water Resources Research*, 51(12), 10008-10028.

464 Brown, V. A., McDonnell, J. J., Burns, D. A., & Kendall, C. (1999). The role of event water, a
465 rapid shallow flow component, and catchment size in summer stormflow. *Journal of*
466 *Hydrology*, 217(3-4), 171-190.

467 Chen, Z., Govindaraju, R. S., & Kavvas, M. L. (1994a). Spatial averaging of unsaturated flow
468 equations under infiltration conditions over areally heterogeneous fields: 1. Development of
469 models. *Water Resources Research*, 30(2), 523-533.

470 Chen, Z., Govindaraju, R. S., & Kavvas, M. L. (1994b). Spatial averaging of unsaturated flow
471 equations under infiltration conditions over areally heterogeneous fields 2. Numerical
472 simulations. *Water Resources Research*, 30(2), 535-548.

473 Chang, C. H., & Lee, K. T. (2008). Analysis of geomorphologic and hydrological characteristics
474 in watershed saturated areas using topographic-index threshold and geomorphology-based runoff
475 model. *Hydrological Processes: An International Journal*, 22(6), 802-812.

476 Chow, V. T., Maidment, D. R., & Mays, L. W. (1988). *Applied Hydrology* McGraw-Hill Book
477 Company. New York.

478 Chow, V., Maidment, D. R., & Mays, L. W. (1962). *Applied hydrology*. *Journal of Engineering*
479 *Education*, 308, 1959.

480 Dehghanian, N., Saeid Mousavi Nadoushani, S., Saghafian, B., & Damavandi, M. R. (2020).
481 Evaluation of coupled ANN-GA model to prioritize flood source areas in ungauged
482 watersheds. *Hydrology Research*, 51(3), 423-442.

483 Essig, E.T., 2008. Modeling infiltration and deep flow over sloping surfaces, M.S. Thesis, Purdue
484 University, 268 p.

485 Fariborzi, H., Sabzevari, T., Noroozpour, S., & Mohammadpour, R. (2019). Prediction of the
486 subsurface flow of hillslopes using a subsurface time-area model. *Hydrogeology Journal*, 27(4),
487 1401-1417.

488 Foks, S. S., Raffensperger, J. P., Penn, C. A., & Driscoll, J. M. (2019). Estimation of Base Flow
489 by Optimal Hydrograph Separation for the Conterminous United States and Implications for
490 National-Extent Hydrologic Models. *Water*, 11(8), 1629.

491 Harris, D. M., McDonnell, J. J., & Rodhe, A. (1995). Hydrograph separation using continuous
492 open system isotope mixing. *Water Resources Research*, 31(1), 157-171.

493 Hursh, C. R., & Brater, E. F. (1941). Separating storm-hydrographs from small drainage-areas into
494 surface-and subsurface-flow. *Eos, Transactions American Geophysical Union*, 22(3), 863-871.

495 Johst, M., Casper, M. C., Muller, C., & Schneider, R. (2013). Separation of Stormflow
496 Hydrographs in Surface and Subsurface Flow by Perceptual Based Modelling of Channel Inflow
497 Components. *The Open Hydrology Journal*, 7(1).

498 Keshtkaran, P., SABZEVARI, T., & Karami Moghadam, M. (2018). Estimation of runoff in
499 ungauged catchments using the Nash non-dimensional unit hydrograph (Case study: Ajay and
500 Kasilian catchments).

501 Kim, N. W., & Shin, M. J. (2018). Estimation of peak flow in ungauged catchments using the
502 relationship between runoff coefficient and curve number. *Water*, 10(11), 1669.

503 Kim, N. W., Shin, M. J., & Lee, J. E. (2016). Application of runoff coefficient and rainfall-
504 intensity-ratio to analyze the relationship between storm patterns and flood responses. *Hydrology
505 and Earth System Sciences Discussions*, 1-48.

506 Lee, J., Kwak, C., & Park, H. (2015). Estimation of runoff coefficient through infiltration analysis
507 by soil type. *Journal of Korean Society of Hazard Mitigation*, 15(4), 87-96.

508 Lee, K. T., & Chang, C. H. (2005). Incorporating subsurface-flow mechanism into
509 geomorphology-based IUH modeling. *Journal of Hydrology*, 311(1-4), 91-105.

510 Liu, Y. B., & De Smedt, F. (2004). WetSpa extension, a GIS-based hydrologic model for flood
511 prediction and watershed management. *Vrije Universiteit Brussel, Belgium*, 1, e108.

512 Menberu, M.W., Torabi Haghighi, A., Ronkanen, A., Kvaerner, J., Kløve, B., (2014). Runoff
513 Curve Numbers for Peat-Dominated Watersheds. *Journal of Hydrologic Engineering*, 20 (4).

514 Mishra, S. K., & Singh, V. P. (2013). Soil conservation service curve number (SCS-CN)
515 methodology (Vol. 42). Springer Science & Business Media.

516 Morbidelli, R., Saltalippi, C., Flammini, A., Cifrodelli, M., Corradini, C., & Govindaraju, R. S.
517 (2015). Infiltration on sloping surfaces: laboratory experimental evidence and implications for
518 infiltration modeling. *Journal of Hydrology*, 523, 79-85.

519 Morbidelli, R., Saltalippi, C., Flammini, A., & Govindaraju, R. S. (2018). Role of slope on
520 infiltration: a review. *Journal of hydrology*, 557, 878-886.

521 Petroselli A., Grimaldi S. 2018. Design hydrograph estimation in small and fully ungauged basins:
522 a preliminary assessment of EBA4SUB framework. *Journal of Flood Risk Management*, 11: S197–
523 S210.

524 Petroselli, A., Asgharinia, S., Sabzevari, T., & Saghafian, B. (2020a). Comparison of design peak
525 flow estimation methods for ungauged basins in Iran. *Hydrological Sciences Journal*, 65(1), 127-
526 137.

527 Petroselli A. 2020. A generalization of the EBA4SUB rainfall-runoff model considering surface
528 and subsurface flow. *Hydrological Sciences Journal* 65(14), 2390-2401.

529 Petroselli A., Piscopia R., Grimaldi S. (2020b). Design discharge estimation in small and ungauged
530 basins: EBA4SUB framework sensitivity analysis. *Journal of Agricultural Engineering* 2020;
531 LI:1040.

532 Piscopia R., Petroselli A., Grimaldi S. 2015. A software package for the prediction of design flood
533 hydrograph in small and ungauged basins. *Journal of Agricultural Engineering* XLVI:432, 74-84.

534 Ribolzi, O., Patin, J., Bresson, L. M., Latsachack, K. O., Mouche, E., Sengtaheuanghoung, O., &
535 Valentin, C. (2011). Impact of slope gradient on soil surface features and infiltration on steep
536 slopes in northern Laos. *Geomorphology*, 127(1-2), 53-63.

537 Robinson, J. S., & Sivapalan, M. (1996). Instantaneous response functions of overland flow and
538 subsurface stormflow for catchment models. *Hydrological processes*, 10(6), 845-862.

539 Rodriguez-Iturbe, I. and Valdes, J.B. (1979) The geomorphologic structure of hydrologic
540 response. *Water Resour. Res.*, 15 (6), 1409–1420.

541 Sabzevari, T., Fattahi, M. H., Mohammadpour, R., & Noroozpour, S. (2013). Prediction of surface
542 and subsurface flow in catchments using the GIUH. *Journal of Flood Risk Management*, 6(2), 135-
543 145.

544 Sabzevari, T., & Noroozpour, S. (2014). Effects of hillslope geometry on surface and subsurface
545 flows. *Hydrogeology journal*, 22(7), 1593-1604.

546 Sabzevari, T. (2017). Runoff prediction in ungauged catchments using the gamma dimensionless
547 time-area method. *Arabian Journal of Geosciences*, 10(6), 131.

548 Singh, V. P. (1988). *Hydrologic systems. Volume I: Rainfall-runoff modeling*. Prentice Hall,
549 Englewood Cliffs New Jersey. 1988. 480.

550 Tarboton, D. G. (2003). *Rainfall-runoff processes*. Utah State University, 1(2).

551 Tekeli, Y. I., & ŞORMAN, Ü. (2003). Separation of Hydrograph Components Using Stable
552 Isotopes Case Study: The Güvenç Basin, Ankara. *Turkish Journal of Engineering and
553 Environmental Sciences*, 27(6), 383-396.

554 Tiefan, P., Jianmei, L., Jinzhong, L., & Anzhi, W. (2005). A modified subsurface stormflow model
555 of hillsides in forest catchment. *Hydrological Processes: An International Journal*, 19(13), 2609-
556 2624.

557 Troch, P. A., Mancini, M., Paniconi, C., & Wood, E. F. (1993). Evaluation of a distributed
558 catchment scale water balance model. *Water Resources Research*, 29(6), 1805-1817.

559 Wels, C., Cornett, R. J., & Lazerte, B. D. (1991). Hydrograph separation: a comparison of
560 geochemical and isotopic tracers. *Journal of Hydrology*, 122(1-4), 253-274.

561